Ecological Interface Design for Solar Car Strategy: From State Equations to Visual Relations.

Antony Hilliard, Greg A. Jamieson, *Member, IEEE*

***Abstract*—Renewable energy technologies present a distinct set of challenges for human problem solving and decision making. Solar car racing typifies opportunities for Human Factors Engineering to support human performance in renewable energy domains, for example through computer interface design. Derivational and topographical adequacy are introduced as useful considerations to guide development of Representation-Aided interfaces and system instrumentation requirements. Implications for generalizability to emerging renewable energy applications are discussed.**

I. Introduction

Industrialized nations face an uncertain energy future. Threats such as global warming and anticipated scarcity of hydrocarbon fuels present a problem to long-term planning efforts [1]. Renewable energy has been recognized as part of a solution; wind, solar, small hydro-, tidal, wave, and biomass technologies are receiving steadily increasing investment, though their contribution to global energy supply remains small [2]. Transportation systems in particular are almost exclusively powered by nonrenewable energy sources.

While research into renewable energy technologies has focused on optimizing technical performance, human interaction with these systems may prove equally important. The complexities inherent in renewable energy systems resemble those seen in other safety-critical systems that challenge human control (or that of mixed teams of humans and automation). For example, renewable energy systems are particularly *open to external disturbances*, which can be inherently unpredictable. Because of lower energy densities, they must be *highly distributed*, with many installations over a large area. In combination with their dynamic energy sources, these characteristics result in *uncertainty* in measurement and prediction of system states. Finally, the operation of renewable energy systems is often *subject to time pressures* imposed by energy distribution requirements [3]. Given that systems with these characteristics have historically been susceptible to catastrophic failure [4], it is prudent to consider the implications these technologies will have for human work.

Manuscript received March 16th, 2007. This work was supported in part by a grant from the National Science and Engineering Research Council.

Antony Hilliard is with the Department of Mechanical and Industrial Engineering, University of Toronto, ON, M5S 3G8, Canada (e-mail: anthill@mie.utoronto.ca).

Greg A. Jamieson is also with the Department of Mechanical and Industrial Engineering, University of Toronto, ON, M5S 3G8, Canada (phone: 1-416-946-8504 e-mail: jamieson@mie.utoronto.ca).

An example of a renewable energy application is the sport of solar car racing, which for the past two decades has showcased the evolution of photovoltaic energy and electric transportation technology. As in other motorsports, optimizing racecar performance is a team's main objective. When competitors have equally matched race cars, however, superior team strategy in both planning and decision-making can be the deciding factor in victory.

Solar race strategy cannot be pre-planned due to complexities typical of renewable energy systems. Chaotic disturbances in the race environment such as clouds, wind, precipitation, and traffic have strong and unpredictable influences on the car. Races span entire continents, and with eight hours of daily racing take nearly a week to complete. Because of these uncertainties, a strategy group of two to four people must accompany the solar car in a chase van for the duration of the race. From the tight confines of this vehicle they continuously adapt the team's race strategy to changing conditions by integrating data from weather forecasts, telemetry, and car physics computer models. Developing and maintaining a planned race speed profile that optimizes car average speed while balancing risks of the dynamic race environment is cognitively demanding and has many time pressures. The tools available to strategy group typically consist of single-sensor-single-indicator telemetry readouts, car physics models with command-line input, and paper printouts of equipment performance curves. A base of expertise in strategy planning is difficult to develop for most teams due to the infrequency of competitions and turnover of team members as students complete their studies.

Similarly complex systems have historically benefited from improvements in safety, reliability, and performance through Human Factors design interventions such as computer interfaces. This paper discusses the design of a Solar Racing Strategy support tool prototype for the University of Toronto BlueSky Racing team.

II. Approach

In managing the complexities of solar car racing, the strategy group has several needs that an interface design should address: 1) support for efficiently reasoning about the complexities of the car's energy supply, conversions, and losses, 2) support for timely detection and diagnosis of a wide variety of equipment malfunctions, including unexpected events, and 3) accessibility by non-expert users, and help for such users in developing expertise. Underlying these three

objectives is a need for availability of relevant system information.

One interface design technique that has been explicitly developed to support these three objectives is Ecological Interface Design (EID) [5], the most well-developed of the family of Representation Aiding (or Semantic Mapping) approaches [6]. Many case studies demonstrating applications of EID in energy-related domains have been discussed in the literature [7-13] and in pedagogical texts [14]. However, no publications have yet discussed EID's applicability to the distinct set of challenges characteristic of distributed renewable energy domains.

Identifying relevant system information for EID is achieved through a Work Domain Analysis (WDA), capturing key domain relationships with structure that guides application to design [4, 15]. A WDA generates multiple functional representations of the system, mirroring the levels of abstraction that humans employ when solving complex problems [16]. The strategy group's tasks, for example, require them to consider highly concrete elements such as physical wear on car components, highly abstract purposes such as safety and race victory, as well as concepts at intermediate levels of abstraction such as car maneuvering capability or motor electrical efficiency.

Cognitive work can be supported at all levels of abstraction by presenting relevant information in intelligible forms. As an example, to address a car mechanical failure, the strategy group will need to determine quickly and accurately whether safety necessitates an immediate halt, or if it will be quicker to "live with" the problem and fix it at the next race stage stop. Decisions cannot be based solely on detection of a physical or functional problem; to paraphrase Rasmussen, "keep racing – don't stop and look for the loose wire" [16].

To ensure that an interface can support workers' activities over a broad range of system states including rare abnormal conditions, EID principles stipulate that interfaces should highlight relationships that remain constant throughout changes in system state. This often means that natural physical laws and engineering equations used to design the system must be included in the interface as perceptual analogies.

When abstract elements are included in an interface, concern should be taken to ensure the adequacy of the concrete measurements used to derive them. Missing or poorly located sensors can dramatically reduce an interface's usefulness, or worse yet, render it misleading [17]. Two relevant considerations discussed in this paper are topographical and derivational adequacy [18]. Topographical adequacy refers to the *location* of a sensor – for example, a light sensor mounted on the chase van may not be an adequate measurement of the light energy hitting the solar racecar's photovoltaic array if the two vehicles are distant from one another. Similarly, derivational adequacy refers to the *quality* of assumptions in a higher level calculation – for example, to calculate the gravitational potential energy of the racecar using only an altimeter, assumptions must be made for the gravitational constant and the mass of the car. Minimizing the number of assumptions and ensuring their validity in abnormal system states helps maintain derivational adequacy. By considering the information requirements identified by a WDA, analysts can *specify* an adequate system sensor set, a clear Human Factors implication for system design [19]. While this paper emphasizes principled application of analysis to design, it must be noted that the design process itself was iterative. Conflicts between instrumentation and interface design choices were encountered, and examples are discussed below.

III. Display Description

Four displays were developed to cover the range of information identified in the solar car racing WDA: navigation, which focused on planned speed and road environment; safety, covering car handling capability and driver fatigue measures; mechanical, featuring detailed instrumentation data on a mimic diagram; and energy, which will be discussed here (see Fig. 1).

Some design choices were determined by the context of the application, in this case, use of laptop computers in a moving vehicle during daytime hours. This working environment suggested that large font sizes, high contrast, and support for navigation through a conventional desktop windowing GUI was desired. As these interface properties can be selected relatively independently of multivariate graphical forms and their arrangement into displays, we will not discuss them in depth. Instead, for a selection of the energy display's graphical forms in Fig. 1, we will discuss their correspondence with mathematical descriptions of the system, and how sensor adequacy concerns affected system or interface design.

The equations used in this discussion contain both simplifying assumptions and altered numerical values to obscure the specifications of the solar car. They are intended to support discussion of the interface design process, not to assert analytical completeness.

A. Solar Intensity

The solar car's sole energy input is the solar radiation striking its photovoltaic array. Using the definitions from Table I, this can be approximated as

$$P_{SI}(t) \cong I(t) \times A. \quad (1)$$

Solar intensity *I(t)* varies primarily with time of day and obstructions such as cloud cover. Array area should remain constant, so long as effects of car orientation and the curves of the solar car's bodyshell are small.

The effects of cloud obstructions on solar intensity were represented in the navigation display, so only a summary of predicted solar irradiative power as it related to energy flows was presented in the energy display. Due to the potential for disturbances, solar predictions were not considered adequate and a solar radiation sensor was identified as a necessary data

source.

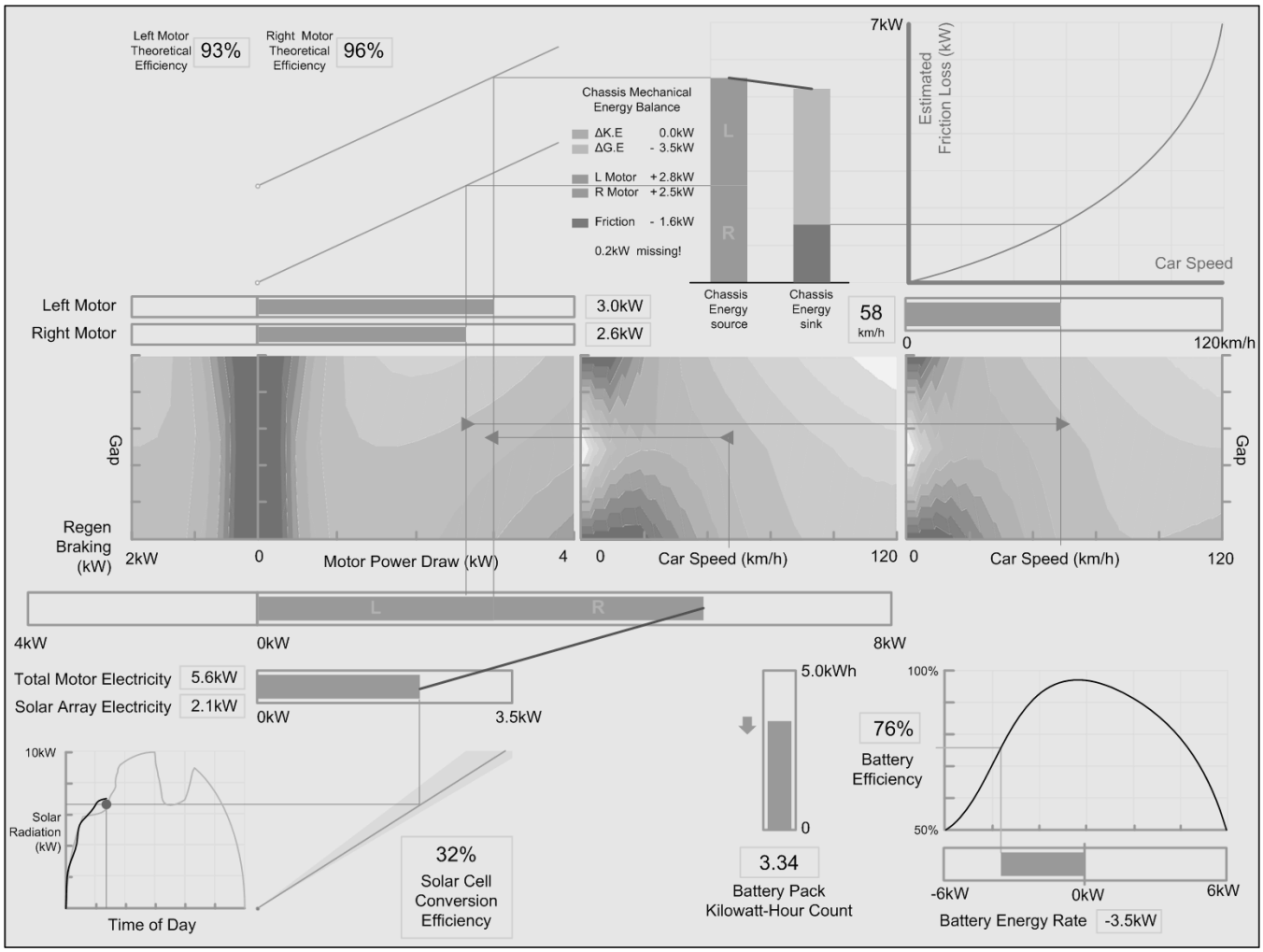

Fig. 1. Prototype Solar Race Strategy 'Energy' Display, describing the solar car's current state in terms of sources, stores, flows, and sinks of energy.

High topographical adequacy could be obtained by integrating the sensor into the solar car array, but at a cost of maintenance accessibility, displacement of solar cells, and aerodynamic penalties. However, race regulations require the chase van to follow immediately behind the solar car, a separation of only a few seconds at normal driving speeds, and solar obstructions such as clouds change more slowly over time scales of minutes. Installing a solar radiation sensor on the chase van was therefore identified as an acceptable alternative option.

The graphical form, shown at the bottom left of Fig. 1, represents the relationship between time of day and the calculated and expected solar irradiative power. The history of values derived from sensor data is displayed with higher salience than predictions, to indicate prominence. Fig. 1 shows that the current solar irradiative power is slightly more than 6kW, that this matches the computed prediction, and that solar intensity is expected to increase rapidly over the next hour, presumably due to cloud dissipation. Connecting lines from the current operating point increase visual proximity to the adjacent solar efficiency form.

B. *Solar Array Conversion Efficiency*

The percent of irradiative power that a solar array converts to electricity is primarily a function of equipment capabilities, but is also influenced by changes in temperature and dust accumulation on the array. Data from array cell temperatures and power electronics sensors were included in the maintenance display, but their relations were nonlinear and difficult to model. This derivational inadequacy discouraged the design of higher-level forms based on these sensors.

The array conversion efficiency η_S can also be found by

$$\eta_S(t) = P_{SE}(t) / P_{SI}(t) \quad (2)$$

where P_{SI} is the solar irradiative power, described in (1) and P_{SE} is the electrical power produced by the solar cells (discussed below in (3)). Deviations from a 'normal' efficiency provide an indirect indicator of the performance of the solar array and power electronics.

A linear 'reflector' form [20] was adopted, and is shown in the bottom center of Fig. 1. The slope of this form corresponds by trigonometric relation to (2), and linking lines emphasize this rise over run relationship. A lightly shaded

wedge-shaped background represents the normal efficiency range. When efficiency decreases and the 'reflector' deviates from this shaded range, increased contrast and form disruption should increase salience and draw attention to the discrepancy. Fig. 1 shows a conversion efficiency of 32%, which in the context of the shaded region indicates good performance.

TABLE I
EXCERPT OF SOLAR CAR PROCESS VARIABLES

Symbol	Definition	Unit	Measured
A	Solar array effective area	m^2	√
A_d	Car frontal drag area	m^2	√
m	Mass of car, including driver	kg	
h	Elevation of car (rel. to race finish)	m	√
g	Gravitational const. at earth surface	m/s^2	
$g_{LM}(t)$	Left motor rotor-stator air gap	mm	√
$g_{RM}(t)$	Right motor rotor-stator air gap	mm	√
$v(t)$	Solar car speed (ground-relative)	km/h	√
$v_w(t)$	Wind speed parallel to road (ground relative)	km/h	√
C_d	Aerodynamic drag coefficient	-	
C_{rf}	Rolling friction coefficient	-	
ρ	Air Density	kg/m^3	√
F_N	Force acting normal to car wheels	N	
$I(t)$	Solar radiation intensity	W/m^2	√
$P_{SI}(t)$	Solar irradiative power	W	
$P_{SE}(t)$	Solar array electrical power	W	
$P_{BE}(t)$	Battery electrical power	W	
$P_{Eloss}(t)$	Electrical resistance losses	W	
$P_{LME}(t)$	Left motor electrical power	W	
$P_{RME}(t)$	Right motor electrical power	W	
$P_{LMW}(t)$	Left motor mechanical power	W	
$P_{RMW}(t)$	Right motor mechanical power	W	
$P_{FW}(t)$	Combined air and rolling friction	W	
$\eta_S(t)$	Solar array efficiency	-	
$\eta_{LM}(t)$	Left motor efficiency	-	
$\eta_{RM}(t)$	Right motor efficiency	-	

C. Electric Energy balance and flow

The electrical energy generated by the racecar's solar arrays is normally consumed by twin electric motors and in minor electrical losses. Battery storage absorbs or supplies any imbalance. Using the definitions in Table I,

$$P_{SE}(t) = P_{LME}(t) + P_{RME}(t) + P_{BE}(t) + P_{Eloss}(t). \quad (3)$$

Because the components of (3) are DC electric power, their values can be calculated with high topographical and derivational adequacy using current and voltage sensors and the relationship P=VI.

Connected bar graphs shown in the lower center of Fig. 1 describe this energy balance. The range of the top bar graph shows that the left and right motors' P_{LME} and P_{RME} can either be positive (consuming electricity to propel the car) or negative (slowing the car and generating electricity via regenerative braking). Since the motors act in parallel on the electrical system and car body, their visual representations were summed. Array electrical power P_{SE} can only be positive, so its bar graph's limits were set accordingly while maintaining the same scale as the motors'. Since battery electric power can be positive or negative, and since increasing values of P_{BE} are associated with increasing electrochemical energy losses, it was instead represented implicitly as the difference between P_{SE} and the summed motor power. A high salience connection line emphasizes the electrical efficiency benefits of a balance between electrical power generation and consumption. Fig. 1 shows that the car's motors are currently consuming over twice the power delivered by the solar arrays, requiring energy input from the batteries.

D. Motor Efficiency Map

Ultra high-efficiency electric motors can either propel the solar car by converting electrical power into mechanical work, or slow it by performing this conversion in reverse as regenerative brakes. The conversion efficiency can be influenced by on-the-fly mechanical adjustment of the motors' rotor-stator separation air gap and is also a function of electrical power input and motor speed. Because the motors are built into the solar car's wheels, their rotational speeds are essentially equal and directly proportional to the car's speed. For the left motor (or the right motor with substitutions from Table I), conversion efficiency is

$$\eta_{\mathrm{LM}}(t) = \frac{P_{LMW}(t)}{P_{LME}(t)} = f\left(g_{LM}(t), P_{LME}(t), v(t)\right). \quad (4)$$

While P_{LME} and P_{RME} can be accurately calculated (3), the motor performance function *f()* must be numerically estimated from test-bed measurements [21]. This represents a source of derivational inadequacy as the motors' condition may deteriorate during a race, causing deviations from predicted performance. To provide a more derivationally and topographically adequate measure of P_{LMW} and P_{RMW}, torque sensors could be added to each motor. However, installing more components inside the compact wheel-motors would not only be costly, it could increase the wheel width and the car's aerodynamic drag. Racecar performance was deemed a priority, so the empirically determined *f()* was used. To communicate its potential derivational weakness, digital displays were captioned 'theoretical efficiency'.

The resulting motor efficiency form is shown in the center of Fig. 1. Three contour graph forms[1] were required to capture the four-dimensional motor performance function (4), and were each based on the instantaneous value of one variable: $v(t)$ for the left graph, P_{LME} for the center, and P_{RME} for the right. Motor gap, as the most independently adjustable variable, provided a common vertical axis. The leftmost plot shares the electrical power balance (3) horizontal axis thus

[1] Contour graphs are three dimensional, with two spatial dimensions and one dimension of shading. True three-dimensional visualizations are difficult for humans to interpret and should usually be avoided.

showing its relation to motor electrical power (4). The current operating point of each motor is indicated with a triangular icon, and linked to increase visual proximity.

This display supports the strategy group in supervising the driver's operation of the motors. Higher efficiency gap settings for the car's current speed or motor power can be directly perceived as lighter contours above or below the current operating point, and increasing efficiency correlates with increased contrast between the operating point icon and the background. Fig. 1 shows that the motors' gap settings are not optimal at this speed, and that they should both be increased.

E. Speed – Friction Energy Relation

Friction energy losses are composed of aerodynamic drag and rolling resistance. The first increases geometrically with wind-relative vehicle speed, and the other directly with ground-relative vehicle speed:

$$P_{FW}(t) \cong 0.5\rho A_d C_d \left(v(t) - v_w(t)\right)^3 + F_N C_{rf}\, v(t)\,. \quad (5)$$

Drag coefficients such as A_dC_d and C_{rf} (described in Table I) must be empirically determined, while instrumentation on the solar car and chase vehicle can measure ρ, v, v_w and normal force[2]. These terms have limitations: A_dC_d and C_{rf} are determined for a well-functioning car with no crosswind, and v_w must be measured on the chase van due to the drag introduced by wind sensors. The resulting P_{FW} therefore has only moderate topographical and derivational adequacy, and its inclusion should be carefully considered. Three justifications can be made for its inclusion. The first was the difficulty of measuring friction losses. Friction losses are very uncertain, and any relation that reduces a portion of the uncertainty leaves less for the strategy group to consider with respect to 'normal' (as discussed below in (6)). The second was the implications of errors in P_{FW}. Because of the ideal conditions under which drag coefficients are determined, calculated drag should tend to underestimate actual drag. This suggests that using (5) to monitor for unexpected energy sinks will result in false alarms rather than misses. While false alarms may cause extra diagnostic workload for the strategy group, misses are more directly harmful to race performance. Thirdly, inaccurate measurements of vehicle drag present few risks to safety. Equation (5) was thus included, with the label 'estimated' to indicate its uncertainty.

The resulting energy relationship is visualized at the top right of Fig. 1. By sharing the horizontal car velocity axis and linking with vertical lines to the right-most (4) contour map, the form corresponds with the physical influence of car velocity on both motor efficiency and friction losses. The effects of the other variables in (5) are included implicitly, meaning that the curve shape will change with changes in air density, wind, or normal force. Because of the high level of integration in this form, (5)'s variables were also included separately in maintenance and safety displays.

F. Mechanical Energy balance

The solar car's body is subject to conservation of mechanical energy, in a balance similar to that of (3). Physical processes such as acceleration and hill climbing can be represented as rates of change of kinetic ($1/2mv^2$) and gravitational potential (mgh) energy:

$$P_{LMW}(t) + P_{RMW}(t) \cong mv(t)\frac{dv}{dt} + mg\frac{dh}{dt} + P_{FW}(t) \quad (6)$$

Motor power, kinetic, and gravitational potential energy rates (see Table I) are positive when the car is accelerating and climbing, and negative when the car is decelerating, using regenerative brakes, and descending a hill. Since a fixed vehicle weight is mandated by race regulations, only vehicle speed and altitude sensors are needed to derive kinetic and potential energy changes[3] with good topographical and derivational accuracy.

The resulting chassis energy balance graphical form is found at the top center of Fig. 1, and uses a connected and summed bar graph similar to (3). Contributions to mechanical energy input (left bar) and removal (at right) are distinguished with color and shading, since every element of (6), with the exception of friction, can either transfer energy to or from the car body. Such changes in polarity, for example in potential energy as the solar car reaches the crest of a hill, would appear as the light grey bar in the right column shrinking to zero, then reappearing in the left hand column as the car begins a descent. This behavior avoids the inconsistency of a summed bar graph containing both positive and negative elements. A line connects the source and sink bar graphs, and others link motor mechanical power and friction energy bars to representations of (4) and (5), respectively.

Unaccounted-for energy flow is represented by the connecting line's slope, which should be of interest to the strategy group as it captures effects of a wide range of possible equipment malfunctions that may only become apparent later from other sensor data. The proximity and relevance of neighboring graphical forms allows abstract questions concerning energy and speed to be considered visually. For example, Fig. 1 shows that roughly two-thirds of motor output is being converted to gravitational potential energy, and that approximately 200W is missing from the power balance. Following the height of the energy sink bar to its intercept with the speed-friction curve, it can be seen that the car will reach 110 km/h if current motor power is maintained after the hill climb is completed.

Such flexibility in display interpretation can be expected to support the strategy team in a wide range of situations that were not foreseen by designers.

[2] These measurements are made by an air density sensor, a motor speedometer, a ground speed-corrected wind sensor in the chase vehicle, and travel sensors on solar car suspension, respectively.

[3] Accelerometers could further increase adequacy by measuring fore/aft acceleration as well as road incline angle.

IV. Discussion

This paper illustrates typical interface and sensor design choices faced in a Representational Aiding design process. Once relevant expressions of physical laws and engineering relationships have been identified, topographical and derivational adequacy must be considered before specifying sensors and developing graphical forms.

The energy display's abstract representation of the solar car's processes provides an externalized mental model for the strategy team. This should support the strategy group in fault diagnosis, and help in interpreting data from other displays. By reducing the cognitive demands of such behavior, this interface should support less experienced group members and free cognitive resources for other tasks.

Renewable energy systems such as wind turbines are governed by the same physical laws as solar cars. While the solar car converts electrical energy into air motion, wind turbines essentially perform the reverse. The invariance of physical laws suggests that the motor efficiency map of (4), the wind power transfer form of (5), and the energy balance of (6) may be applicable to other renewable energy domains.

The personnel responsible for operating and maintaining renewable energy installations have many of the same responsibilities as the solar car strategy team: anticipating and evaluating the effects of disturbances, identifying potential maintenance issues in a timely and accurate fashion, and optimizing financial and energy performance. For low energy density renewable energy technologies to be adopted widely enough to significantly contribute to societal energy demands, non-expert people may be required to assume responsibility for equipment operation and maintenance. Human Factors design interventions have the potential to contribute to adoption of renewable technology by reducing its cognitive demands.

Verifying these assertions will require significant investigation. While EID-inspired displays have consistently demonstrated their benefits to human control and adaptation, the solar car interface has not yet been evaluated in an applied setting. Generalizing to other renewable energy domains presents another opportunity for future research.

V. Conclusions

In systems which are governed by physical laws, engineering system representations can be useful to system operators. By designing computer interfaces to include abstract representations of the processes underlying system behavior, human problem-solving, monitoring, and expertise can be supported. Visual representations must be designed with care, ensuring that they are supported by adequate instrumentation.

Renewable energy systems are attracting increasing investment and interest as fossil fuel costs and risks continue to increase. Representation-Aided interfaces provide flexible tools that may help support the human element in an effective widespread adoption of renewable energy systems.

Acknowledgement

The authors acknowledge the BlueSky Race Team, Brandon Wang, Joe Crampton, and Matthew Ying for their contributions to the interface design, as well as Nathan Lau for his thoughtful reviews.

References

[1] S. N. Stern. 2006, *The Economics of Climate Change.* [Online]. Available: http://www.hm-treasury.gov.uk/independent_reviews/stern_review_economics_climate_change/sternreview_index.cfm

[2] REN 21. 2006, *Renewables Global Status Report 2006 Update.* [Online]. Available: http://www.ren21.net/

[3] National Energy Board. 2006, *Emerging Technologies in Electricity Generation - an Energy Market Assessment.* (1st ed.) [Online]. Available: http://www.neb-one.gc.ca

[4] K. J. Vicente, *Cognitive Work Analysis : Toward Safe, Productive, and Healthy Computer-Based Work.* Mahwah, N.J.: Lawrence Erlbaum Associates, 1999, pp. 392.

[5] K. J. Vicente and J. Rasmussen, "Ecological interface design: Theoretical foundations," *IEEE Trans Syst Man Cybern,* vol. 22, pp. 589-606, 1992.

[6] K. B. Bennett, A. L. Nagy and J. M. Flach, "Visual displays," in *Handbook of Human Factors and Ergonomics* ,3rd ed.G. Salvendy, Ed. Hoboken, NJ: Wiley, 2006, pp. 1191-1219.

[7] J. Itoh, A. Sakuma and K. Monta, "Ecological interface for supervisory control of BWR nuclear power plants," *Control Engineering Practice,* vol. 3, pp. 231-239, 1995.

[8] C. M. Burns, "Putting it all together: Improving display integration in ecological displays," *Hum. Factors,* vol. 42, pp. 226-241, 2000.

[9] Y. Yamaguchi and F. Tanabe, "Energy balance in a reactor system," in *Proceedings of the XIVth Triennial Congress of the International Ergonomics Association and the 44th Annual Meeting of the Human Factors and Ergonomics Society,* 2000, pp. 571-574.

[10] D. H. Ham and W. C. Yoon, "The effects of presenting functionally abstracted information in fault diagnosis tasks," *Reliab Eng Syst Saf,* vol. 73, pp. 103-119, 2001.

[11] R. Memisevic, P. Sanderson, S. Choudhury and B. -. W. Wong, "Work domain analysis and ecological interface design for hydropower system monitoring and control," in *Proceedings of the 2005 IEEE International Conference on Systems, Man and Cybernetics,* 2005, pp. 3580-3587.

[12] N. Lau and G. A. Jamieson, "Ecological Interface Design for the Condenser Subsystems of a Boiling Water Reactor," in *Proceedings of the 16th World Congress on Ergonomics*, 2006, (no pagination).

[13] J. Kwok and C. M. Burns, "Ecological Interface Design for the Turbine Subsystem of a Boiling Water Reactor," in *Proceedings of the 16th World Congress on Ergonomics*, 2006, (no pagination).

[14] C. M. Burns and J. R. Hajdukiewicz, *Ecological Interface Design.* Boca Raton, Florida: CRC Press, 2004, pp. 307.

[15] J. Rasmussen, A. M. Pejtersen and L. P. Goodstein, *Cognitive Systems Engineering.* New York: Wiley, 1994, pp. 378.

[16] J. Rasmussen, *Information Processing and Human-Machine Interaction : An Approach to Cognitive Engineering.* , vol. 12, New York: North-Holland, 1986, pp. 215.

[17] D. V. C. Reising and P. M. Sanderson, "Work domain analysis and sensors II: Pasteurizer II case study," *Int J Hum Comput Stud,* vol. 56, pp. 597-637, 2002.

[18] D. V. C. Reising and P. M. Sanderson, "Minimal instrumentation may compromise failure diagnosis with an ecological interface," *Hum. Factors,* vol. 46, pp. 316-333, 2004.

[19] K. J. Vicente, K. J. Christoffersen and C. N. Hunter, "Response to Maddox critique." *Hum. Factors,* vol. 38, pp. 546, 1996.

[20] W. S. Pawlak and K. J. Vicente, "Inducing effective operator control through ecological interface design," *Int J Hum Comput Stud,* vol. 44, pp. 653-688, 1996.

[21] N. Lau, "Numerical models in representation design: Computing seawater properties in an ecological interface," in *Proceedings of the Human Factors and Ergonomics Society 50th Annual Meeting,* 2006, pp. 245-249.